Journal of Power Sources 194 (2009) 920–930

Contents lists available at ScienceDirect

Journal of Power Sources

journal homepage: www.elsevier.com/locate/jpowsour

Control of a heat-integrated proton exchange membrane fuel cell system with methanol reforming

Wei Wu*, Che-Chuan Pai

Department of Chemical and Materials Engineering, National Yunlin University of Science and Technology, Douliou, Yunlin 64002, Taiwan, ROC

ARTICLE INFO

Article history:
Received 6 March 2009
Accepted 18 May 2009
Available online 23 May 2009

Keywords:
Fuel processing
Proton exchange membrane fuel cell
Heat integration
Multi-loop control

ABSTRACT

This work presents a novel heat-integrated fuel cell stack system with methanol reforming. Its configuration is composed of fuel processing units (FPUs), proton exchange membrane (PEM) fuel cell stack, and heat exchangers (HEXs). Well mixed methanol and oxygen flows in contact with countercurrent flowing water dominates the production of hydrogen at the exit of FPUs and influences the stack temperature. The heat exchange connections can enhance the utilization of energy of FPUs. To ensure the stable steady-state operation, the model-free fuzzy incremental control scheme within the multi-loop feedback control framework is developed. Finally, the proposed system integration and control configuration are verified by closed-loop simulations.

1. Introduction

Fuel cells are widely recognized as one of the most promising clean energy technologies of the future. The proton exchange membrane (PEM) fuel cell is quite suitable for residential or automotive applications [1], for the following reasons. (i) It can operate at a relatively low temperature; (ii) it has relatively high power density; (iii) its maintenance is simple. However, the efficiency of the PEMFC is strongly affected by the unsteady hydrogen feed flow, cell temperature, membrane dehydration and fast variations in load. Developing a source of pure hydrogen is a commercial challenge. Liquid hydrocarbons such as methanol, ethanol, and gasoline are usually treated as alternative hydrogen-rich fuel streams [2]. Notably, the methanol-fuelled reformer has been widely studied for fuel cell applications.

Toward the development of a fuel reforming system, Lindstrom and Pettersson [3] presented a compact methanol reformer for fuel cell vehicles; Lattner and Harold [4] developed a kinetic reactor model for autothermal reforming of methanol; Stamps and Gatzke [5] modeled the packed-bed methanol reformer; Choi and Stenger [6] proposed an integrated methanol reformer system to study the hydrogen yield and economic profit, and Wang and Wang [7] used a thermodynamic and exergetic analysis of a PEMFC stack system with methanol reforming. Recently, Xu et al. [8] explored the energy efficiency of a methane reforming system with heat integration. In fact, the methane-fuelled reforming system has been inadequately incorporated into the PEMFC system because of restrictions on operating temperature and pollutant emissions. In our opinion, an integrated power generation system should depend on the synergy between heat integration and control design.

With respect to the fuel cell control problem, Lauzze and Chmielewski [9] provided a set of feedback structures, including power, temperature and relative humidity controllers; Woo and Benziger [10] showed that the proportional-integral-derivative (PID) control could accelerate the response of a PEMFC system to satisfy the load demand; Methekar et al. [11] adopted the multi-input multi-output (MIMO) PI control framework to control of the power density and temperature of a distributed parameter model of fuel cell systems, and Wu et al. [12] indicated that the MIMO control structure can ensure the highly efficient control performance when a low-order and simplistic model of the PEMFC systems is considered. However, the models-based predictive control schemes are adopted to improve the control performance by using the fuzzy Hammerstein model [13] or neural network techniques [14]. Moreover, fuzzy control schemes [15,16] and fuzzy neural networks [17] have been successfully applied to many fuel cell systems.

This article introduces the kinetics and modeling of fuel processing units (FPUs), including a methanol reformer (MR), heat exchangers (HEX), a water gas shift (WGS) reactor, and a preferential oxidation (PROX) reactor. In the proposed system configuration, the inlet methanol flow can influence the amount of hydrogen produced, and the countercurrent flow of water by virtue of heat exchange connections can improve energy utilization and regulate the stack temperature. Furthermore, the multi-loop fuzzy incremental control framework ensures the satisfactory tracking performance and reliability of the proposed heat-integrated system according to the closed-loop simulation.

* Corresponding author.
E-mail address: weiwu@yuntech.edu.tw (W. Wu).

0378-7753/$ – see front matter.
doi:10.1016/j.jpowsour.2009.05.030

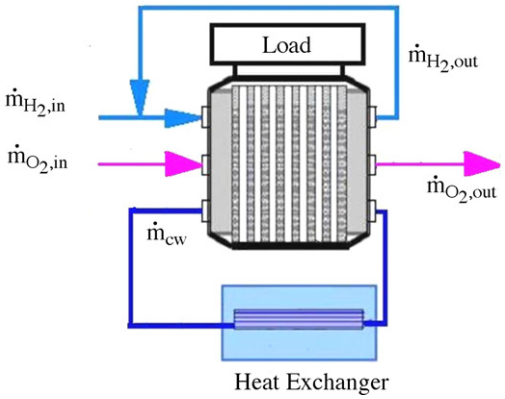

Fig. 1. Individual PEMFC stack system with cooling device.

2. PEMFC stack system

A Ballard 5 kW PEMFC stack system was constructed using the empirical-type model [18,19], which consists of 35 cells in series. Regarding the individual PEMFC stack system shown in Fig. 1, pure hydrogen is fed to the anode, excess hydrogen gas is re-circulated, and the stack temperature is changed by a heat exchange system with circulating water.

2.1. Anode and cathode flow models

Based on the assumption that all gases are ideal, the principles of mole conservation can be used to model the reactant flows at the anode and the cathode:

$$\begin{aligned}\frac{V_a}{RT}\frac{dP_{H_2}}{dt} &= \dot{n}^{FC}_{H_2,in} - k_a(P_{H_2} - P_{amb}) - \frac{nI}{2F}\\ \frac{V_c}{RT}\frac{dP_{O_2}}{dt} &= \dot{n}^{FC}_{O_2,in} - k_c(P_{O_2} - P_{amb}) - \frac{nI}{4F}\end{aligned} \tag{1}$$

where $\dot{n}^{FC}_{H_2,in}$ and $\dot{n}^{FC}_{O_2,in}$ are the hydrogen and oxygen inlet mole flow-rates, respectively. Notably, the inlet hydrogen flow-rate usually varies with the amount of hydrogen supplied, and the oxygen flow-rate can be determined by multiplying the air inlet flow-rate by the mole fraction of oxygen in air (21%).

2.2. Thermal model

The energy balance of the stack system is determined by the total power converted by the fuel H_2 into electricity, the power consumed by the electrical load, the rate of heat removal by the coolant, $\dot{Q}_{cool}$, and the rate of heat loss at the stack surface, $\dot{Q}_{loss}$. The dynamic model is described by a couple of first-order differential equations:

$$\begin{aligned}C_t\frac{dT}{dt} &= \dot{E}_{tot} - \dot{E}_{elec} - \dot{Q}_{loss} - \dot{Q}_{cool}\\ \rho_w V_w C_{pw}\frac{dT_{c,out}}{dt} &= \dot{m}_{cw}C_{pw}(T_{c,in} - T_{c,out})\\ &+UA\left(T - \frac{T_{c,in}+T_{c,out}}{2}\right)\end{aligned} \tag{2}$$

where

$$\begin{aligned}\dot{E}_{tot} &= \frac{nI}{2F}\Delta H\\ \dot{E}_{elec} &= V_{stack}I\\ \dot{Q}_{loss} &= \frac{C_t(T - T_{amb})}{\tau}\\ \dot{Q}_{cool} &= (h_{cond} + h_{conv}I)\frac{(T - T_{c,in}) - (T - T_{c,out})}{\ln((T - T_{c,in})/(T - T_{c,out}))}\end{aligned} \tag{3}$$

$T_{c,in}$ and $T_{c,out}$ are the inlet and outlet water temperatures, respectively. $\dot{m}_{cw}$ is the mass flow-rate of water; ρ_w is the density of water; V_w is the volume of the heat exchange system, and T is the stack temperature.

2.3. Polarization curve model

The polarization curve is generally used to specify the relation between the cell voltage V_{fc} and current density I. When a cell delivers power to the load, the load voltage E is reduced by the voltage drop, comprising of the activation overvoltage V_{act} and the ohmic overvoltage V_{ohm}. The output voltage of a single fuel cell is given by

$$V_{fc} = E - V_{act} - V_{ohm} \tag{4}$$

(i) The open-circuit cell potential E is, as determine by the Nernst equation, given by

$$E = 1.229 - 8.5\times10^{-4}(T - 298.15) + \frac{RT}{2F}\ln[P_{H_2}(P_{O_2})^{0.5}] \tag{5}$$

(ii) With respect to the dynamics of the activation overvoltage V_{act}, the first-order dynamic accounting for the effects of double layer capacitance charging at the electrode-electrolyte interfaces is described by

$$\frac{dV_{act}}{dt} = \frac{I}{C_{dl}} + \frac{E_{act}}{R_{act}C_{dl}} \tag{6}$$

where the activation resistance $R_{act} = V_{act}/I$; the activation drop E_{act} is defined by

$$E_{act} = \beta_1 + \beta_2 T + \beta_3 T\ln(C_{O_2}) + \beta_4 T\ln(I), \tag{7}$$

and the parametric coefficients $\beta_1, \ldots, \beta_4$ are expressed as

$$\begin{aligned}\beta_1 &= -0.948\\ \beta_2 &= 0.00286 + 0.0002\ln(A_{fc}) + 4.3\times10^{-5}\ln(C_{H_2})\\ \beta_3 &= 7.6\times10^{-5}\\ \beta_4 &= -1.93\times10^{-4}\end{aligned} \tag{8}$$

with

$$\begin{aligned}C_{O_2} &= 1.97\times10^{-7}P_{O_2}\exp\left(\frac{498}{T}\right)\\ C_{H_2} &= 9.174\times10^{-7}P_{H_2}\exp\left(\frac{-77}{T}\right)\end{aligned} \tag{9}$$

Notably, C_{O_2} is the oxygen concentration at the cathode/membrane interface and C_{H_2} is the hydrogen concentration at the anode/membrane interface.

(iii) The ohmic overvoltage is given by,

$$V_{ohm} = IR_{int} \tag{10}$$

where the internal resistance R_{int}, obtained by the empirical analysis, is written as,

$$R_{int} = \frac{r_M l_m}{A_{fc}} \tag{11}$$

and the membrane resistivity r_M is given by

$$r_M = \frac{181.6[1 + 0.03(I/A_{fc}) + 0.062(T/303)^2(I/A_{fc})^{2.5}]}{[11.866 - 3(I/A_{fc})]\exp[4.18((T - 303)/T)]} \tag{12}$$

According to Eqs. (1)–(12), a single fuel cell is affected by current density, cell temperature, hydrogen and the partial pressure of oxygen. Table 1 presents parameter definitions and values of a Ballard 5 kW PEMFC stack system. Since all cells are in series, the total voltage for the stack is given by

$$V_{stack} = 35V_{fc} \tag{13}$$

Table 1
Parameter definitions and values of the Ballard MK5-E system.

Parameter	Description	Value
V_a	Anode volume (m^3)	0.005
k_a	Anode flow constant ($mol\,s^{-1}\,atm^{-1}$)	0.065
$\dot{n}^{FC}_{H_2,in}$	Hydrogen inlet flow-rate ($mol\,l^{-1}$)	0.8
P_{amb}	Ambient pressure (atm)	1
V_c	Cathode volume (m^3)	0.01
k_c	Cathode flow constant ($mol\,s^{-1}\,atm^{-1}$)	0.065
$\dot{n}^{FC}_{O_2,in}$	Oxygen inlet flow-rate ($mol\,s^{-1}$)	2
F	Faraday constant ($C\,mol^{-1}$)	96,485
ΔH	Hydrogen enthalpy of combustion ($kJ\,mol^{-1}$)	285.5
C_t	Thermal capacitance ($kJ\,°C^{-1}$)	17.9
h_{cond}	Parameter for conduction property of heat exchanger ($W\,°C^{-1}$)	35.55
h_{conv}	Parameter for convection property of heat exchanger ($W\,°C^{-1}\,A^{-1}$)	0.025
T_{amb}	Ambient temperature (°C)	25
$T_{c,in}$	Inlet water temperature (°C)	25
UA	Stack heat transfer coefficient ($W\,K^{-1}$)	241
C_{pw}	Heat capacity of water ($kJ\,kg^{-1}\,K^{-1}$)	4.184
ρ_w	Water density ($kg\,m^{-3}$)	1000
V_w	Volume of the cooling system (m^3)	2.5×10^{-3}
τ	Time constant	2.06
A_{fc}	Effective cell area (cm^2)	232
l_m	Membrane thickness (cm)	178×10^{-4}
R	Universal gas constant ($J\,mol^{-1}\,K^{-1}$)	8.314
C_{dl}	Double layer capacitance (F)	0.035×232
λ	Membrane resistivity parameter	12.5

2.4. Simulation and analysis

The Simulink™ was used to simulate the PEMFC stack system whose structure is given in Appendix A.1. Fig. 2 shows that, when the current is step changed from 0.5 to 45 A at the time 20 min, the stack temperature obviously arises and may cause the membrane dehydration when the temperature exceeds 170 °C. If ±5% step changes of $\dot{m}_{cw}$ are considered in Eq. (2), then the variation of the mass flow-rate of water induces the asymmetric responses of the stack temperature, as shown in Fig. 3. In both figures, the circulating water flow clearly affects the temperature of the stack system.

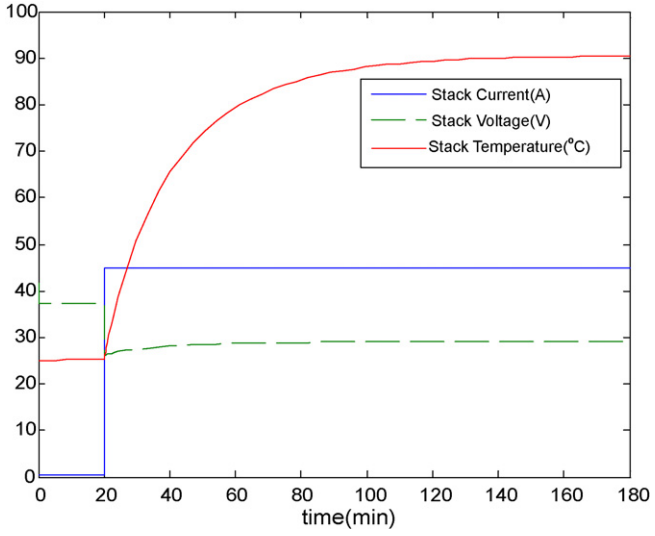

Fig. 2. Open-loop responses of voltage and temperature of the PEMFC stack system when the step change of the current appears.

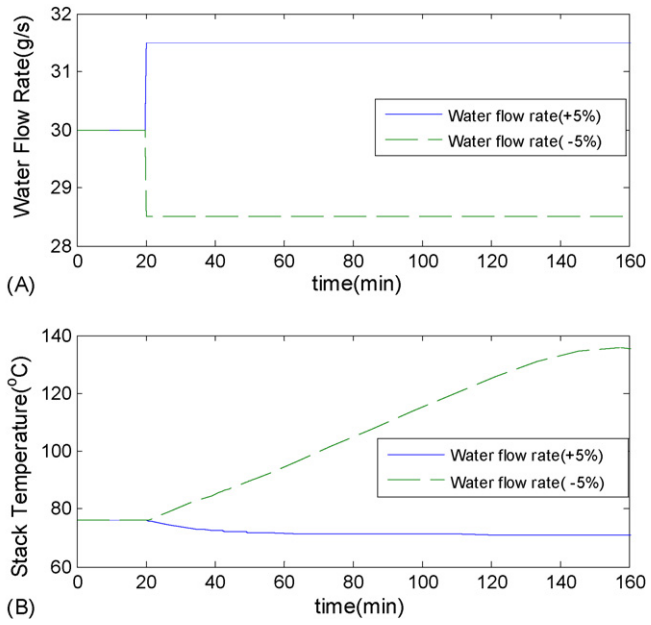

Fig. 3. Open-loop responses of the PEMFC stack system: (A) the step change of water flow-rate; (B) corresponding stack temperature.

3. Fuel processing units

3.1. Unit connections

FPUs mainly consist of HEXs, an MR system, a WGS reactor, and a PROX reactor. Their dynamics are simplified using ideal-gas models. In an MR system, water and methanol flows are well mixed to proceed the steam reforming, and an excess amount O_2 (air) is added to satisfy the demand for partial oxidation of methanol (POM). The equation of continuity for species in a multicomponent reacting mixture can be used to determine the exit mole flow-rates of components $\dot{n}^{MR}_{H_2}$, $\dot{n}^{MR}_{CO}$ and $\dot{n}^{MR}_{H_2O}$ according to specified reaction rates in Eqs. (B1)–(B3) under prescribed inlet conditions and catalyst weights in Table 2. Since CO is produced by direct decomposition of methanol, a mixture of CO and H_2O takes part in the reversible exothermic reaction, known as a water-gas shift reaction, to produce hydrogen and reduce the concentration of CO. The reaction of the WGS system is described in Appendix B and the exit mole flow-rates of components $\dot{n}^{WGS}_{H_2}$, $\dot{n}^{WGS}_{CO}$, $\dot{n}^{WGS}_{CO_2}$ and $\dot{n}^{MR}_{H_2O}$ are determined by the following material balances:

$$\begin{aligned}
\dot{n}^{WGS}_{H_2} &= \dot{n}^{MR}_{H_2} + r_{WGS} \\
\dot{n}^{WGS}_{CO_2} &= r_{WGS} \\
\dot{n}^{WGS}_{CO} &= \dot{n}^{MR}_{CO} - r_{WGS} \\
\dot{n}^{WGS}_{H_2O} &= \dot{n}^{MR}_{H_2O} - r_{WGS}
\end{aligned} \tag{14}$$

where the rate of the WGS reaction r_{WGS} is determined by solving Eq. (B4) at the prescribed operating temperature. The outlet flows of the WGS reactor include a small amount of CO, which is typically less than 1%. The selective oxidation reaction of CO in a PROX reactor can

Table 2
Parameter values for fuel processing units.

FPUs	Catalyst (g cat)	Volume (l)
MR	$Cu/ZnO/Al_2O_3$: 100 g (Steam reforming) $Cu/ZnO/Al_2O_3$: 10 g (Partial oxidation of methanol) $Cu/ZnO/Al_2O_3$: 140 g (Methanol decomposition)	10.2
PROX	Pt-Fe/γ-alumina: 40 g	10
WGS	$Cu/ZnO/Al_2O_3$: 100 g	0.5

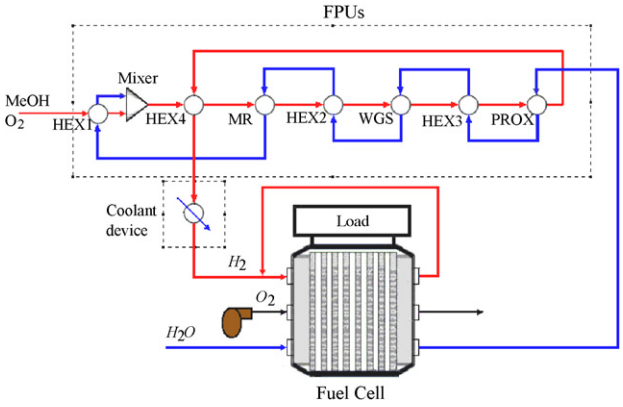

Fig. 4. PEMFC stack system with FPUs and circulating water system.

prevent poisoning of the fuel cell electrodes. Appendix B presents the kinetics of the PROX reactor.

3.2. System integration

In the proposed configuration in Fig. 4, the excess hydrogen gas is circularly fed into the PEMFC stack; methanol is usually selected as an alternative hydrogen-rich fuel stream, and the countercurrent water flow design is employed. In the approach, the original circulating device for cooling the stack system is replaced with external circulating water flow. To ensure the heat-integrated system is compact, and to reduce its heat duty, the FPUs are characterized by the following.

- If the redundant ***perheater or post-combustion unit is omitted, then the heat exchange connections for HEXs aim to improve the energy utilization against the heat duty.
- The countercurrent water flow from the stack to the FPUs plays the role of reactant and heat exchanges.
- A well mixed lowing CH_3OH and O_2 flows comes into contact with the countercurrent water flow, dominating the heat duty and production of hydrogen by each reactor.
- At the exit of the PROX reactor, the amount of hydrogen produced as well as the CO concentration can satisfy the specification of the inlet flow of the PEMFC system.

The calculation of the inlet and outlet temperatures of each reactor depends on the energy balance. Referring the unit connections in Fig. 5, the energy balance of the MR system is expressed as

$$\dot{Q}_1^{in}(T_1^{in}) + \dot{Q}_2^{in}(T_2^{in}) - \dot{Q}_1^{out}(T_1^{out}) - \dot{Q}_2^{out}(T_2^{out}) + \dot{E}_{MR} = 0 \quad (15)$$

where notation '1' stands for the red flow and notation '2' represents the blue flow. $\dot{E}_{MR}$ represents the rate of generation of heat by chemical reactions of the MR system. Assume that all reacting units are denoted as adiabatic steady-state reactor systems. In the PROX system, the flowing water is heated from 298 K at the inlet to an outlet temperature over 373 K, and the latent energy for gasifying the water is given by

$$\dot{Q}_{H_2O}^{out} = \dot{n}_{H_2O}^{PROX}[C_P^{H_2O(l)}(373 - 298) + 44010 + C_P^{H_2O(g)}(T_2^{out} - 373)] \quad (16)$$

Appendix A presents a Simulink^{TM} model of the heat-integrated FPUs. Fig. 6 shows that the inlet and outlet temperatures and the amount of hydrogen produced by each reactor can be individually determined using kinetics and by modeling of every unit, as shown

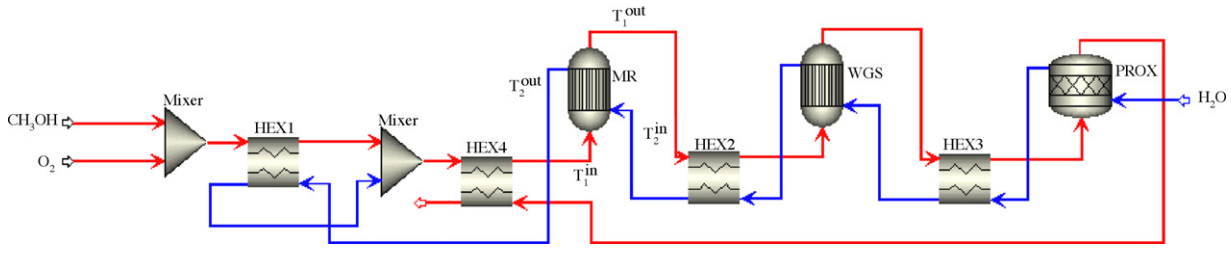

Fig. 5. CH_3OH and O_2 flows come into contact with the countercurrent water flow in FPUs.

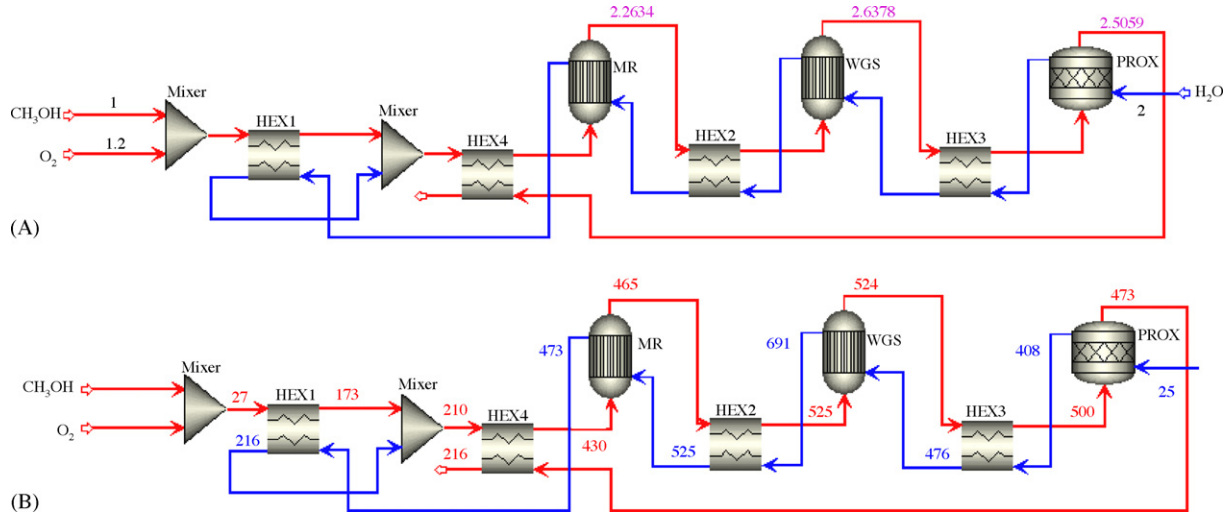

Fig. 6. (A) Specific amount of hydrogen produced at each reactor of FPUs; (B) corresponding temperature at each reactor of FPUs.

Table 3
Parameter values for heat exchanger.

Heat exchanger	Effectiveness (ε)	Volume (l)
HEX1	0.8	0.1
HEX2	0.8	0.1
HEX3	1	0.5
HEX4	0.8	0.1

in Appendix B. In Fig. 6(A), 1 mole CH_3OH with 1.2 mole O_2 (red line) is fed into the mixer point and 2 mole H_2O as the coolant and reactant (blue line) is simultaneously fed into the PROX. The produced hydrogen (over 2.5 mole) exits the PROX reactor as the inlet fuel of the PEMFC stack system. In Fig. 6(B), the inlet and outlet temperatures of FPUs are evaluated with reference to specifications of heat exchangers and the thermodynamic properties of the reactants listed in Tables 2–4. Notably, Eqs. (B7)–(B9) describe the dynamics of HEX for multicomponent inlet and outlet flows. However, the outlet temperature of HEX4 exceeds 80 °C which is inadequate for the feed flow of the PEMFC stack system. Therefore, an extra coolant device is used to cool rapidly the hydrogen flow.

4. Control implementation

Although flowing methanol, oxygen and water are reactants of MR, WGS and PROX reactors, Fig. 7(A) shows that step changes of the inlet water flow-rate obviously change the stack temperature and Fig. 7(B) indicates that step changes in the inlet methanol flow-rate strongly change the hydrogen pressure at the anode. Notably, both flows can be treated as manipulated inputs.

4.1. Fuzzy incremental control design

The model of the proposed heat-integrated power generation system is a simplistic combination, because the dynamic behavior of FPUs is ignored and the PEMFC is an empirical-type model. In fact, the modules in Appendix A are incomplete because Simulink™ blocks do not consider the effects of the condition of the catalyst, mass and heat transfers at the electrodes, the operational limits of the power plant, and balance of plant (BOP) on the electrochemical efficiency [22] are not involved in. Additionally, problems of unmodeled dynamics and model errors are inevitable. In our approach, a model-free fuzzy incremental control is employed because of the PID-like configuration and the sensible tuning gains. Fig. 8(A) depicts the fuzzy incremental control blocks, in which the PD controller output u_n is expressed as

$$u_i = K_p E_i + K_d CE_i \tag{17}$$

where K_p and K_d are tuning parameters, and *error* E_i and *change in error* CE_i represent the inputs of fuzzy logic controller. Using the backward difference, the *change in error* is defined by

$$CE_i = \frac{E_i - E_{i-1}}{T_s} \tag{18}$$

where T_s is the sampling period. The fuzzy logic controller consists of the fuzzy rule (Table 5) and the Λ-type membership function f_Λ. The control structure that is shown in Fig. 8(B) has been proven to generate good results for control applications as well as to be easily implemented in hardware. When two inputs and one output membership were scaled in the [−1,+1] interval, the input–output mappings is specified by a fuzzy inference mechanism with respect to 3×3, 5×5 and 7×7 linguistic variables as displayed in Fig. 9(A–C), respectively. The corresponding control surfaces are more or less bumpy. In Table 5, the fuzzy set of linguistic variables is defined as follows; NB (Negative Big), NM (Negative Medium), NS (Negative Small), ZE (Zero Error), PS (Positive Small), PM (Positive Medium) and PB (Positive Big). Table 5 also indicates the IF–THEN relationship between the membership functions with respect to the linguistic variables for both inputs E_i and CE_i. More-

Table 4
Heat capacity of components of fuel processing units.

Component	Heat capacity (J kg^{-1} K^{-1})
CH_3OH	61.43
O_2	29.4
$H_2O_{(l)}$	75.3
$H_2O_{(g)}$	33.6
CO	29
H_2	28.8
CO_2	43.81

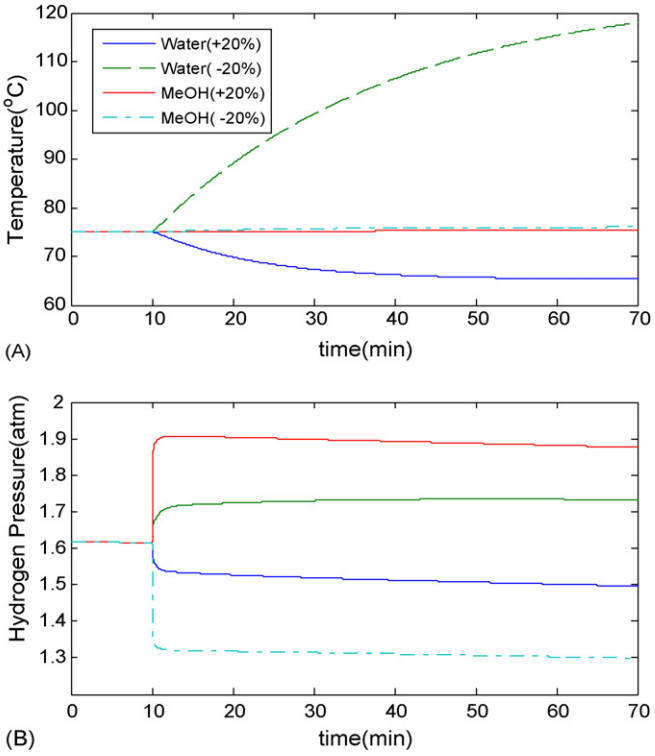

Fig. 7. Open-loop responses of the heat-integrated power generation system with respect to step changes of CH_3OH and H_2O flows: (A) stack temperature; (B) hydrogen pressure at the anode.

Table 5
Symmetric arrangements of fuzzy rule base with respect to 3×3 (blue), 5×5 (red and blue) and 7×7 linguistic variables.

CE_i \ E_i	NB	NM	NS	ZE	PS	PM	PB
NB				**PB**	**PM**	**PS**	**ZE**
NM				**PM**	**PS**	**ZE**	**NS**
NS			**PM**	**PS**	**ZE**	**NS**	**NM**
ZE	**PB**	**PM**	**PS**	**ZE**	**NS**	**NM**	**NB**
PS	**PM**	**PS**	**ZE**	**NS**	**NM**		
PM	**PS**	**ZE**	**NS**	**NM**			
PB	**ZE**	**NS**	**NM**	**NB**			

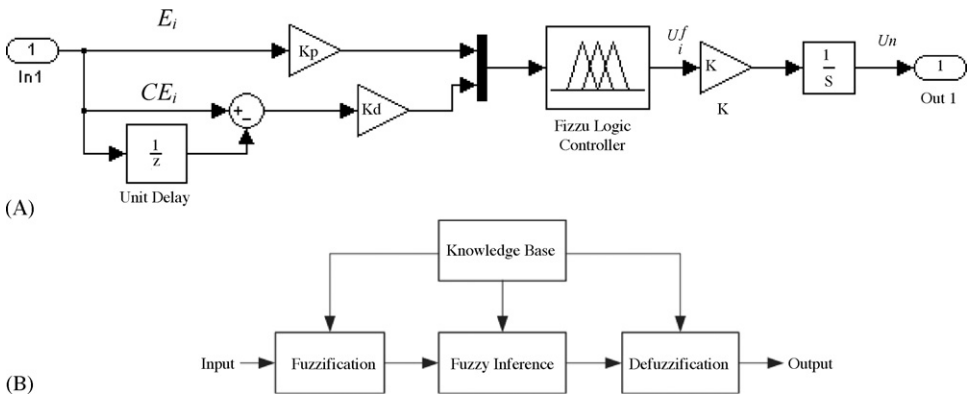

Fig. 8. (A) Simulink™ blocks for the fuzzy incremental controller; (B) fuzzy logic control structure.

over, the output U_i^f of the fuzzy logic controller is written as

$$U_i^f = f_\Lambda(K_p E_i, K_d CE_i) \tag{19}$$

and the fuzzy incremental controller output is expressed as

$$U_n = K_w * \sum_{i=1}^{n} f_\Lambda(K_p E_i, K_d CE_i) * T_s \tag{20}$$

where K_w is the proportional gain. Based on the developments of PID-fuzzy control techniques [23–25], the above structure is similar to a fuzzified proportional-integral-derivative (PID) controller.

4.2. Control effectiveness

To evaluate the effectiveness of PID-fuzzy control, a single-input single-output (SISO) control framework based on the manipulation

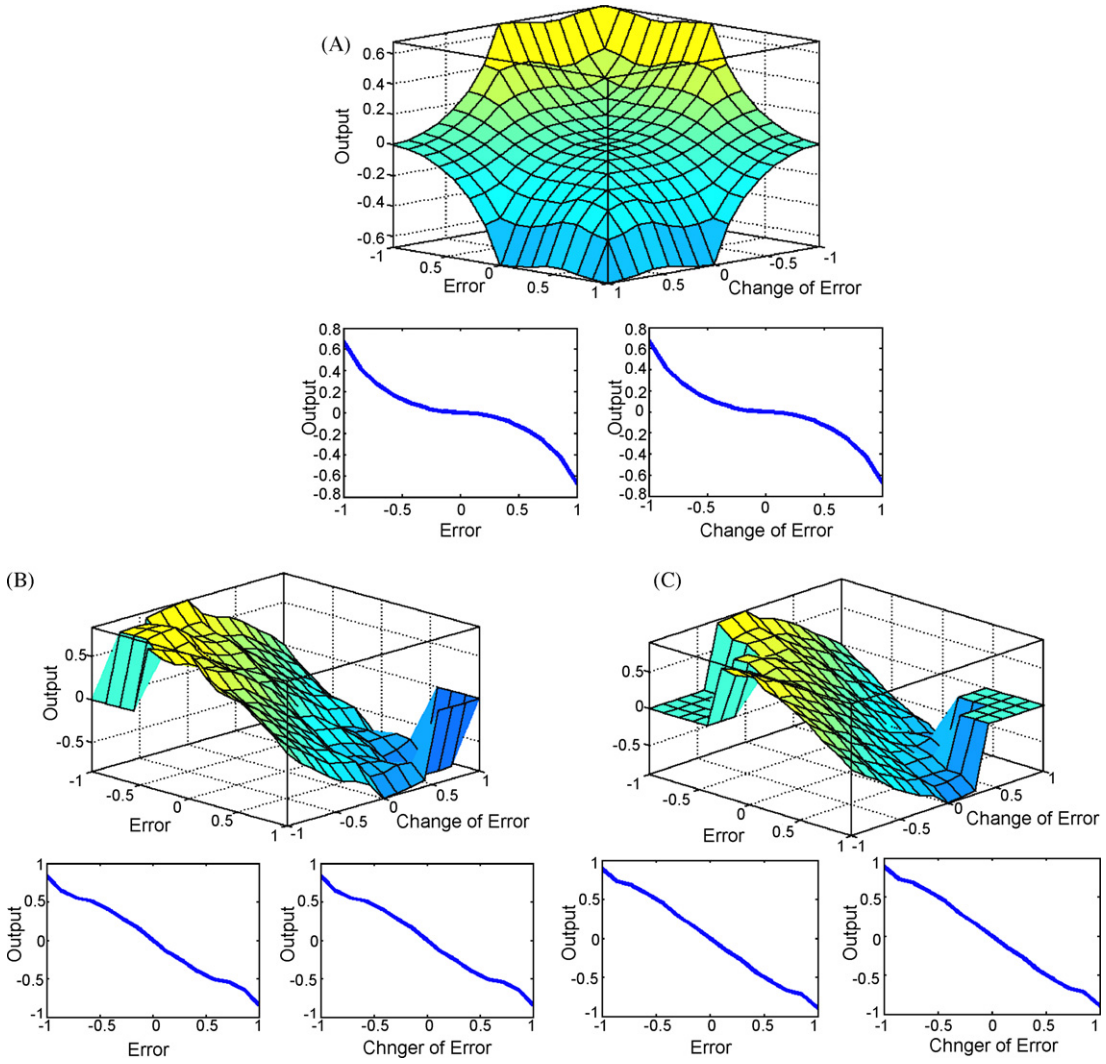

Fig. 9. Plots for the input–output mappings with respect to fuzzy sets: (A) 3 × 3; (B) 5 × 5; (C) 7 × 7.

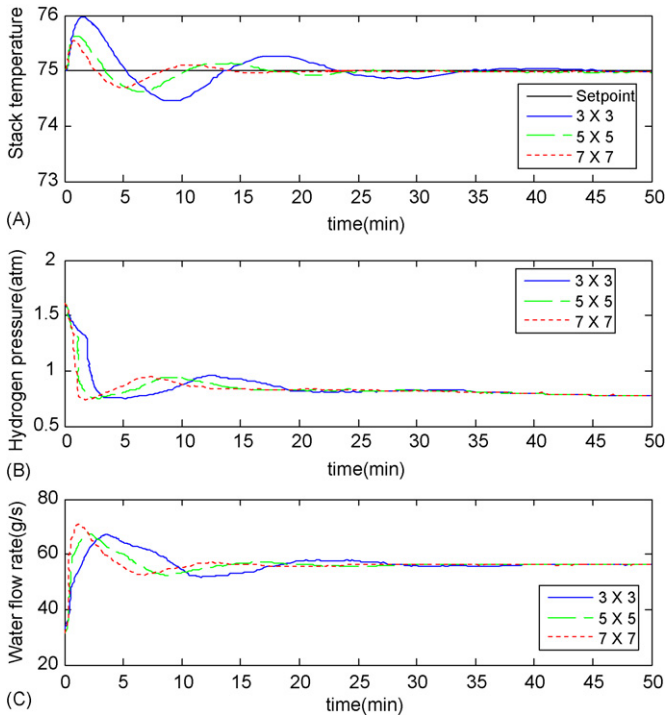

Fig. 10. SISO fuzzy control architecture by tuning parameter K_w: (A) stack temperature; (B) hydrogen pressure at the anode; (C) corresponding manipulation of the water flow-rate.

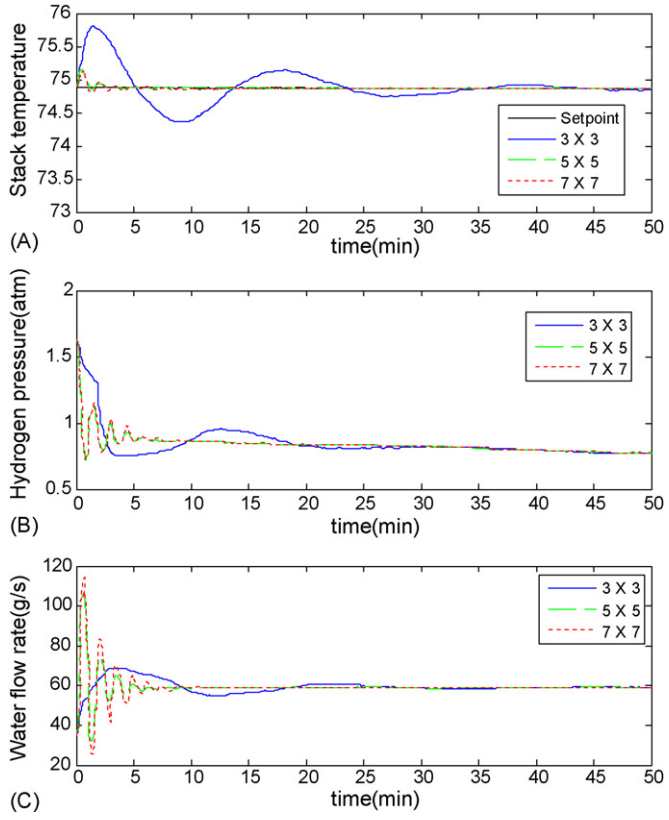

Fig. 11. SISO fuzzy control architecture by alternative fuzzy rule bases: (A) stack temperature; (B) corresponding hydrogen pressure at the anode; (C) corresponding manipulation of the water flow-rate.

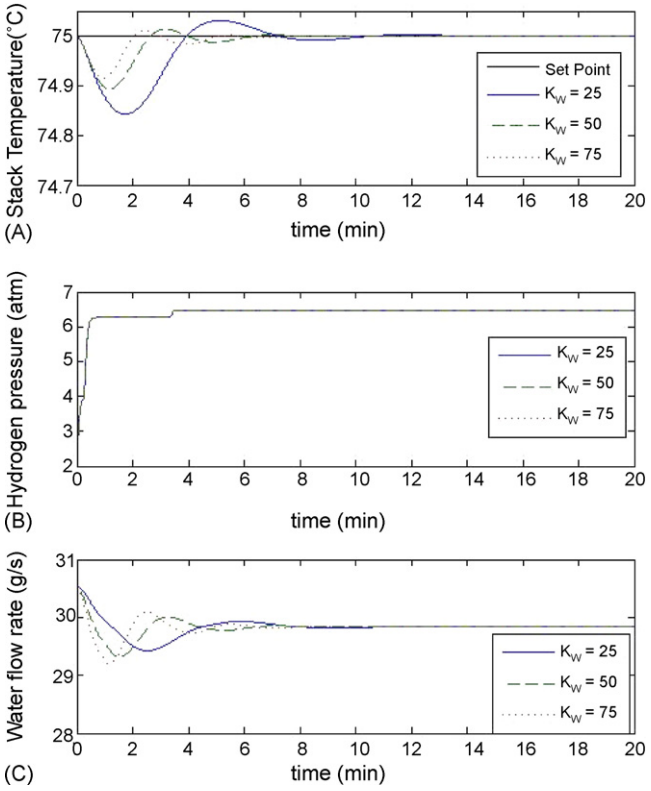

Fig. 12. SISO fuzzy control architecture by tuning parameter K_w for the perturbation of methanol flow at the inlet: (A) stack temperature; (B) hydrogen pressure at the anode; (C) corresponding manipulation of the water flow-rate.

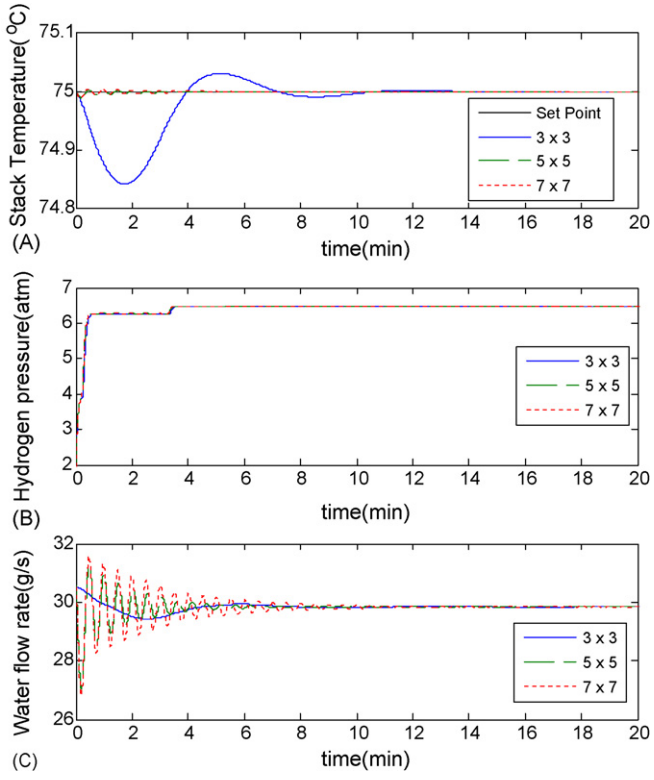

Fig. 13. SISO fuzzy control architecture by alternative fuzzy rule bases for the perturbation of methanol flow at the inlet: (A) stack temperature; (B) hydrogen pressure at the anode; (C) corresponding manipulation of the water flow-rate.

of the single inlet water flow-rate is considered. For fixed parameters $(K_p, K_d) = (0.1, 30)$, Fig. 10(A) shows that when the load demand is initially changed from 40 to 60 A, the stack temperature can be asymptotically regulated at 75 °C by tuning K_w, but the hydrogen pressure, plotted in Fig. 10(B), clearly decrease. Similarly, Fig. 11(A) shows that the stack temperature can be asymptotically regulated at 75 °C using alternative fuzzy rule bases. Notably, the fuzzy sets 5×5 and 7×7 ensure superior output regulation, but the high-gain (rapid) control responses, shown in Fig. 11(C), appear. Fig. 12(A) shows that when the step change of inlet flow-rate of methanol, from 1 to 3 mol s^{-1}, occurs, the stack temperature can be maintained at the desired level by tuning K_w, but the hydrogen pressure, shown in Fig. 12(B), clearly increases. Moreover, Fig. 13 shows that the output regulation of the stack temperature is greatly improved by the use of alternative fuzzy rule bases. According to the aforementioned closed-loop simulations, the stack temperature can be regulated by manipulating the water flow-rate, but the hydrogen pressure at the anode is very sensitive to load changes. Notably, the countercurrent water flow fails to dominate the rate of hydrogen production. The SISO fuzzy control scheme is characterized by the following.

- The alternative fuzzy rule bases can improve the output regulation performance, but they clearly increase the computational burden.
- A single controller parameter by tuning K_w is reliable.
- The SISO control configuration fails to solve the problem since the rate of hydrogen production clearly declines.

To overcome the drawback of the SISO control framework, two fuzzy incremental controllers are implemented to regulate the stack temperature and the hydrogen pressure of the anode by manipulating the inlet flow-rates of both water and methanol. Based on the assumption that the control-loop interaction can be decoupled by the selection of input–output pairings, a multi-loop SISO control configuration is considered. According to the fuzzy control structure in Eq. (20), the controller output for inlet methanol flow-rate is written as

$$\hat{U}_n = K_m \times \sum_{i=1}^{n} f_\Lambda(\hat{K}_p E_i, \hat{K}_d CE_i) \times T_s \tag{21}$$

where K_m is the proportional gain and $\hat{K}_p$ and $\hat{K}_d$ are new tuning parameters. Fig. 14(A) and (B) shows that if the load demand is initially changed from 40 to 60 A, then both stack temperature and the hydrogen pressure can be regulated at the desired levels by tuning one parameter K_m and alternative fuzzy rule bases, respectively. For a positive 75% step change of current, Fig. 15 shows that the controller configurations are employed by tuning K_w and K_m. Notably, both simulation results show that the multi-loops SISO

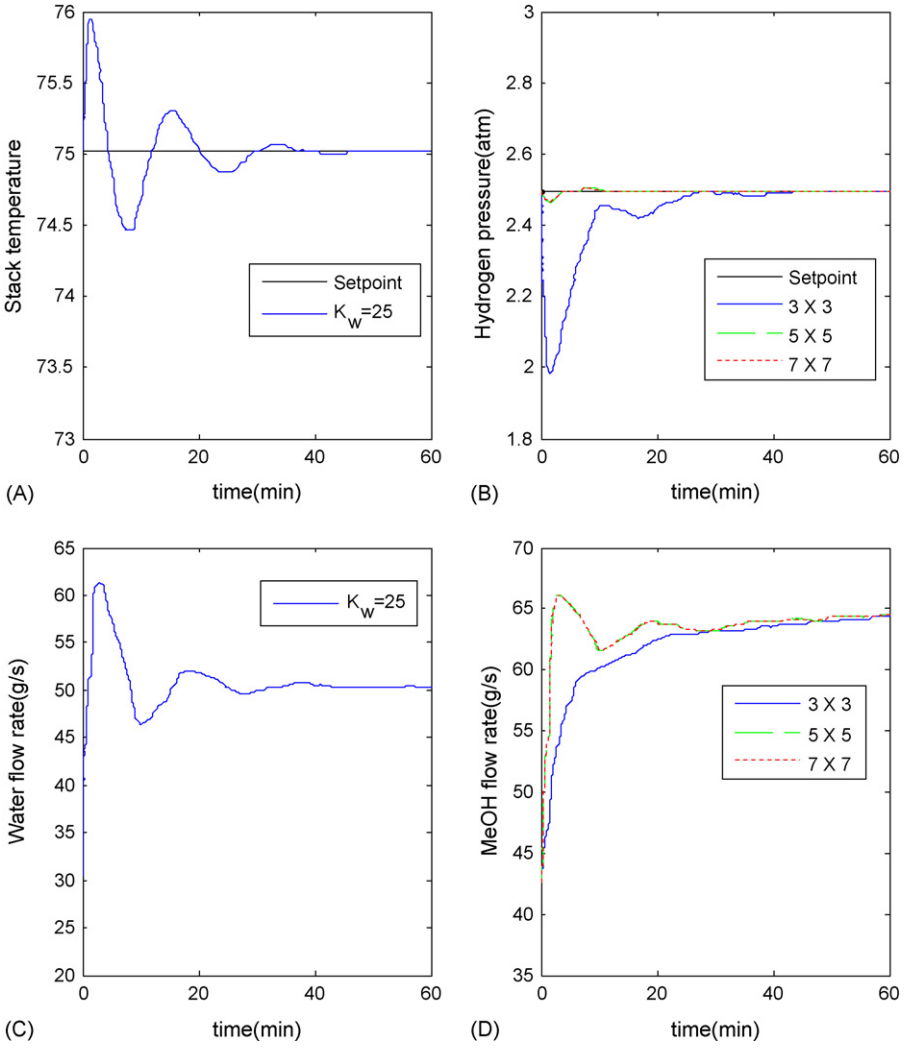

Fig. 14. MIMO fuzzy control architecture by tuning parameter K_w and alternative fuzzy rule bases: (A) stack temperature; (B) hydrogen pressure at the anode; (C) corresponding manipulation of the water flow-rate; (D) corresponding manipulation of the methanol flow-rate.

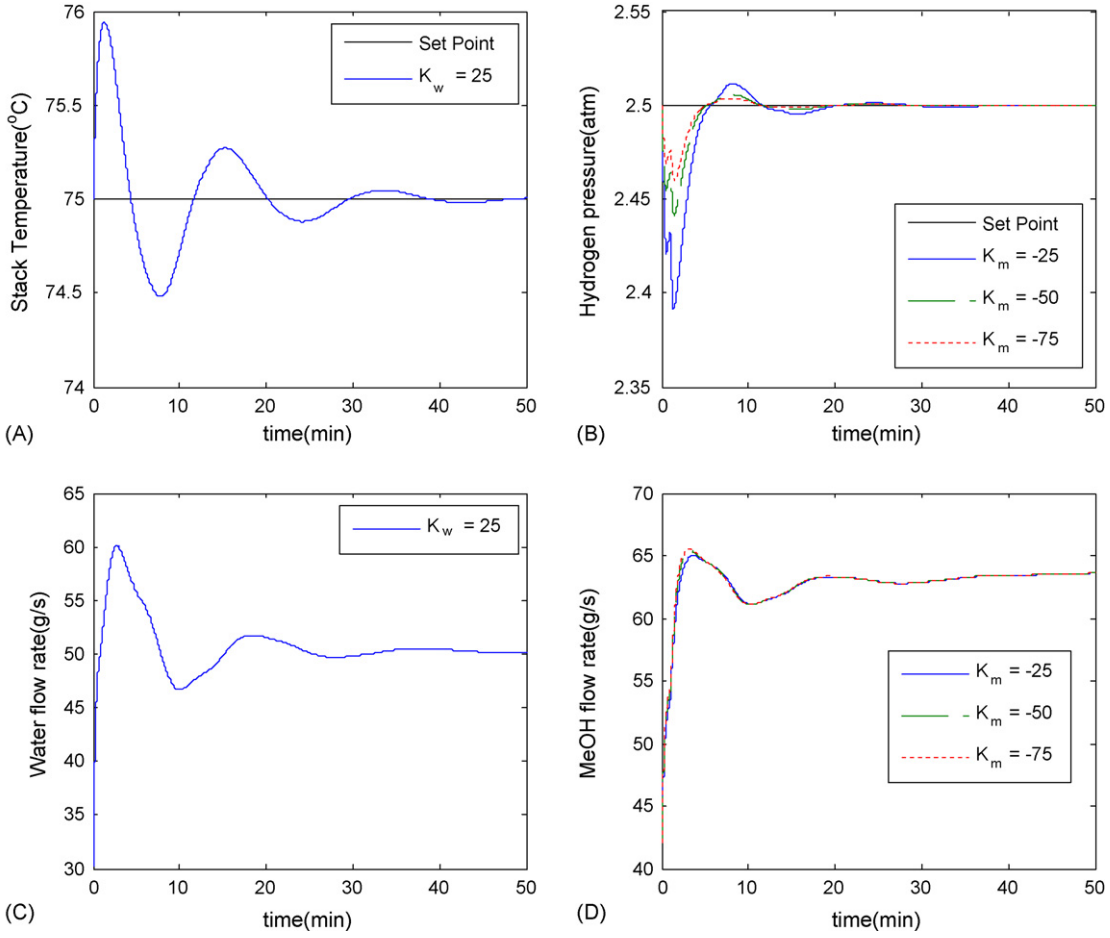

Fig. 15. MIMO fuzzy control architecture by two tuning parameters K_w and K_m for the load change: (A) stack temperature; (B) hydrogen pressure at the anode; (C) corresponding manipulation of the water flow-rate; (D) corresponding manipulation of the methanol flow-rate.

control design guarantees the stable output regulation of a heat-integrated power generation system.

5. Conclusions

In this work, a critical conception and approach from the process system engineering is extended to construct a standalone and valuable power generation system. The heat integration is based on the arrangement of HEXs, the effective mixing of flowing CH_3OH and O_2 at the inlet and countercurrent water flow. Based on the thermodynamic properties and specifications of each reactor of the FPUs, the inlet and outlet temperatures of each reactor and the amount of hydrogen produced at the exit of the PROX reactor can be evaluated using the technical computing software Matlab/Simulink™. Fuzzy incremental control technique within the multi-loop feedback control framework can be applied successfully to ensure the output regulation performance of the heat-integrated power system, in spite of unknown disturbances.

Acknowledgments

The authors would like to thank the National Science Council of the Republic of China for financially supporting this research under Contract No. NSC 97-2221-E-224-018.

Appendix A.

Simulink™ blocks for PEMFC stack and fuel processing subsystems are displayed as follows.

A.1. A grid connected PEMFC stack system

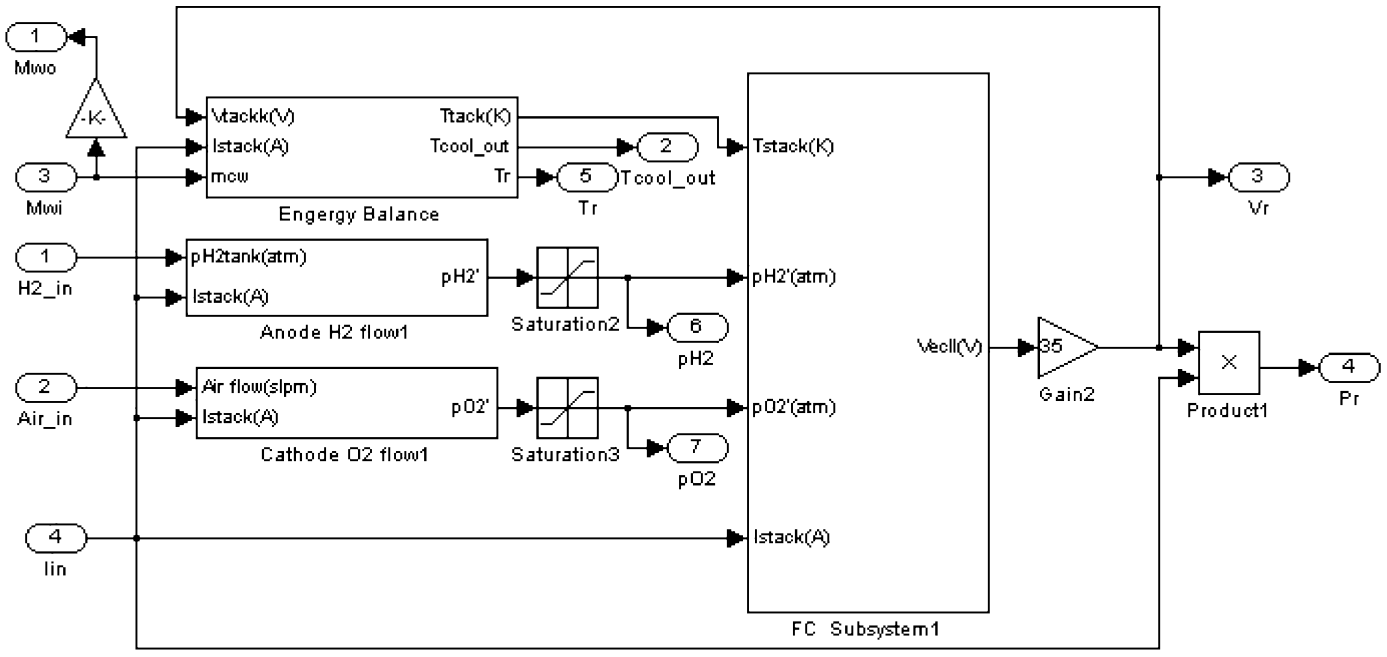

A.2. Heat-integrated fuel processing units

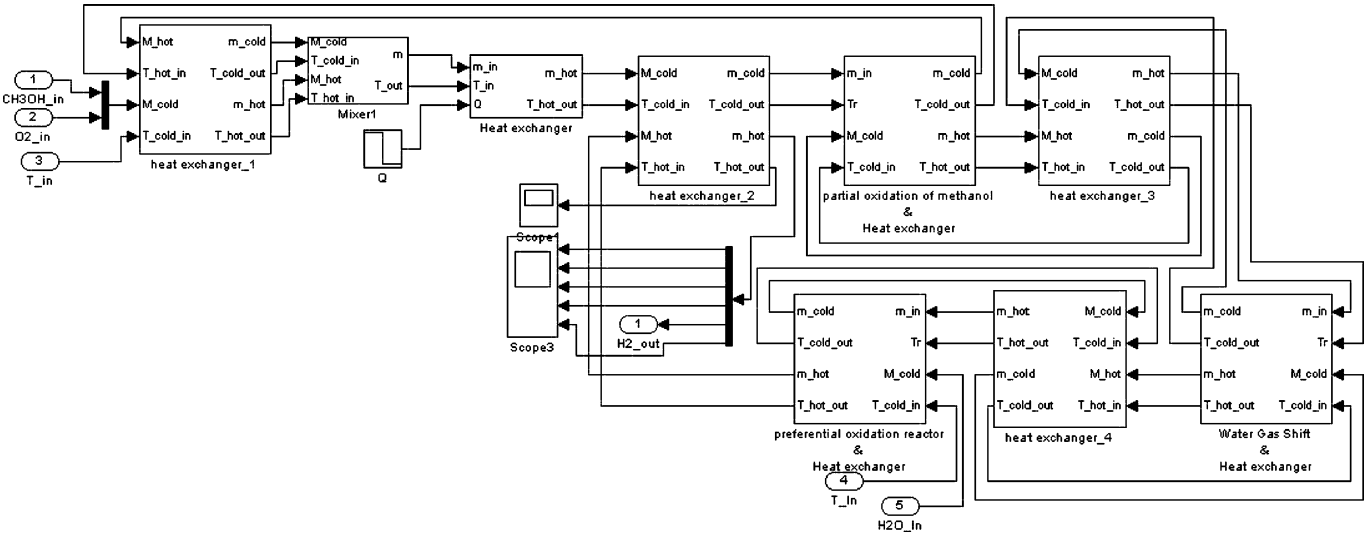

Appendix B.

(i) The kinetics of methanol reformer (MR) include:

Steam reforming

$$\mathrm{MeOH} + \mathrm{H_2O} \overset{\mathrm{Cat}}{\rightleftarrows} \mathrm{CO_2} + 3\mathrm{H_2}, \quad \Delta\hat{H}_R^{\circ} = 49.5\,\mathrm{kJ/mol}$$

and the corresponding reaction rate r_R (mol g cat^{-1} s^{-1}) is shown by

$$\begin{aligned} K_{eq,R} &= 1.849 \times 10^{10} \exp\left(-\frac{56087}{RT}\right) \\ E_{qR} &= 1 - \frac{P_{\mathrm{CO_2}} P_{\mathrm{H_2}}^3}{K_{eq,R} P_{\mathrm{MeOH}} P_{\mathrm{H_2O}}} \\ r_R &= 6.75 \exp\left(-\frac{81000}{RT}\right) P_{\mathrm{MeOH}} E_{qR} \end{aligned} \tag{B1}$$

Partial oxidation of methanol (POM)

$$\mathrm{MeOH} + \tfrac{1}{2}\mathrm{O_2} \xrightarrow{\mathrm{Cat}} \mathrm{CO_2} + 2\mathrm{H_2}, \quad \Delta\hat{H}_R^\circ = -192\,\mathrm{kJ/mol}$$

and the corresponding reaction rate $r_{OX,M}$ (mol g cat^{-1} s^{-1}) is shown by

$$k_{OX,M} = 0.466 \exp\left(-\frac{65000}{RT}\right)$$
$$r_{OX,M} = k_{OX,M} P_{\mathrm{MeOH}} P_{\mathrm{O_2}}^{0.5} \tag{B2}$$

Methanol decomposition (MD)

$$\mathrm{MeOH} \overset{\mathrm{Cat}}{\rightleftarrows} \mathrm{CO} + 2H_2, \quad \Delta\hat{H}_R^\circ = 90.6\,\mathrm{kJ/mol}$$

and the corresponding reaction rate r_D (mol g cat^{-1} s^{-1}) is shown by

$$K_{eq,D} = 1.718 \times 10^{14} \exp\left(-\frac{95418}{RT}\right)$$
$$E_{qD} = 1 - \frac{P_{\mathrm{CO}} P_{\mathrm{H_2}}^2}{K_{eq,D} P_{\mathrm{MeOH}}} \tag{B3}$$
$$r_D = 1.12 \exp\left(-\frac{76000}{RT}\right) P_{\mathrm{MeOH}} E_{qD}$$

(ii) The kinetic of water gas shift (WGS) reactor is described by

$$\mathrm{CO} + \mathrm{H_2O} \overset{\mathrm{Cat}}{\rightleftarrows} \mathrm{CO_2} + 2\mathrm{H_2}, \quad \Delta\hat{H}_R^\circ = -41.15\,\mathrm{kJ/mol}$$

Referring the issue [20], the equilibrium constant K_{WGS} can be expressed as

$$K_{WGS} = \frac{r_{WGS}(\dot{n}_{H_2}^{MR} + r_{WGS})}{(\dot{n}_{CO}^{MR} - r_{WGS})(\dot{n}_{H_2O}^{MR} - r_{WGS})}$$
$$= \exp\left(\frac{5693.5}{T} + 1.077\ln(T) + 5.44 \times 10^{-4} T - 1.125 \times 10^{-7} T^2 - \frac{49170}{T^2} - 13.148\right) \tag{B4}$$

where r_{WGS} (mol g cat^{-1} s^{-1}) represents the reaction rate of WGS reactor.

(iii) The kinetics of preferential oxidation (PROX) reactor include;

CO oxidation

$$\mathrm{CO} + \tfrac{1}{2}\mathrm{O_2} \xrightarrow{\mathrm{Cat}} \mathrm{CO_2}, \quad \Delta\hat{H}_R^\circ = -282.99\,\mathrm{kJ/mol}$$

and the corresponding reaction rate r_{CO} (mol g cat^{-1} s^{-1}) is shown by

$$-r_{CO} = 3.528 \times 10^2 \exp\left(\frac{-33092}{RT}\right) P_{O_2}^{0.5} P_{CO}^{-0.1} \tag{B5}$$

H_2 oxidation

$$\mathrm{H_2} + \tfrac{1}{2}\mathrm{O_2} \xrightarrow{\mathrm{Cat}} \mathrm{H_2O}, \quad \Delta\hat{H}_R^\circ = -285.84\,\mathrm{kJ/mol}$$

and the corresponding reaction rate $r_{\mathrm{H_2}}$ (mol g cat^{-1} s^{-1}) is shown by

$$-r_{\mathrm{H_2}} = 2.053 \times 10^2 \exp\left(\frac{-18742}{RT}\right) P_{\mathrm{O_2}}^{0.5} \tag{B6}$$

(iv) The model of heat exchanger (HEX) is considered as a counter-flow single-pass heat exchanger [21], the outlet temperature of two flows is modeled as

$$\rho_{m_1} C_{pm_1} V_1 \frac{d}{dt} T_1^{out} = \dot{Q}_1^{in} - \dot{Q}_1^{out} - \dot{Q}^{transfer}$$
$$\rho_{m_2} C_{pm_2} V_2 \frac{d}{dt} T_2^{out} = \dot{Q}_2^{in} - \dot{Q}_2^{out} + \dot{Q}^{transfer} \tag{B7}$$

where notation 'm' represents the mean value. $\dot{Q}^{in}$ and $\dot{Q}^{out}$ are the inlet and outlet flows of energy, respectively. The heat capacity of the component is listed in Table 4. The rate of heat transfer $\dot{Q}^{transfer}$ is close to the form of

$$\dot{Q}^{transfer} = \varepsilon C_{\min}(T_1^{in} - T_2^{in}) \tag{B8}$$

where ε represents the heat-exchanger effectiveness, and the minimum heat capacity C_{min} is expressed as

$$C_{\min} = \frac{\dot{m}_1 C_{pm_1} \dot{m}_2 C_{pm_2}}{\dot{m}_1 C_{pm_1} + \dot{m}_2 C_{pm_2}} \tag{B9}$$

References

[1] J.T. Pukrushpan, A.G. Stefanopoulou, H. Peng, Control of Fuel Cell Power Systems, Springer-Verlag, London, 2004.
[2] M. Wang, Fuel choices for fuel-cell vehicles: well-to-wheels energy and emission impacts, J. Power Sources 112 (2002) 307–321.
[3] B. Lindstrom, L.J. Pettersson, Development of a methanol fuelled reformer for fuel cell applications, J. Power Sources 118 (2003) 71–78.
[4] J.R. Lattner, M.P. Harold, Autothermal reforming of methanol: experiments and modeling, Catal. Today 120 (2007) 78–89.
[5] A.T. Stamps, E.P. Gatzke, Dynamic modeling for a methanol reformer-PEMFC stack system for analysis and design, J. Power Sources 161 (2006) 356–370.
[6] Y. Choi, H.G. Stenger, Kinetics, simulation and optimization of methanol steam reformer for fuel cell applications, J. Power Sources 142 (2005) 81–91.
[7] S. Wang, S. Wang, Energy analysis and optimization of methanol generating hydrogen system for PEMFC, Int. J. Hydrogen Energy 31 (2006) 1747–1755.
[8] C. Xu, L.T. Biegler, M.S. Jhon, Systematic optimization of an H_2 PEM fuel cell power generation system with heat integration, AIChE J. 52 (2006) 2496–2506.
[9] K.C. Lauzze, D.J. Chmielewski, Power control of a polymer electrolyte membrane fuel cell, Ind. Eng. Chem. Res. 45 (2006) 4661–4670.
[10] C.H. Woo, J.B. Benziger, PEM fuel cell current regulation by fuel feed control, Chem. Eng. Sci. 62 (2007) 957–968.
[11] R.N. Methekar, V. Prasad, R.D. Gudi, Dynamic analysis and linear control strategies for proton exchange membrane fuel cell using a distributed parameter model, J. Power Sources 165 (2007) 152–170.
[12] W. Wu, J.P. Xu, J.J. Hwang, Multi-loop nonlinear predictive control scheme for a simplistic hybrid energy system, Int. J. Hydrogen Energy 34 (2009) 3953–3964.
[13] F. Jurado, Predictive control of solid oxide fuel cells using fuzzy Hammerstein models, J. Power Sources 158 (2006) 245–253.
[14] L. Zhang, M. Pan, S. Quan, Model predictive control of water management in PEMFC, J. Power Sources 180 (2008) 322–329.
[15] C. Shen, G.Y. Gao, X.J. Zhu, X.J. Sun, Nonlinear modeling and adaptive fuzzy control of MCFC stack, J. Process Control 12 (2002) 831–839.
[16] J.O. Schumacher, P. Gemmar, M. Denne, M. Zedda, M. Stueber, Control of miniature proton exchange membrane fuel cells based on fuzzy logic, J. Power Sources 129 (2004) 143–151.
[17] T. Sun, S.J. Yan, G.Y. Cao, X.J. Zhu, Modelling and control PEMFC using fuzzy neural networks, J. Zheijang Univ. Sci. 6(A) (10) (2005) 1084–1089.
[18] J.C. Amphlett, R.M. Baumert, R.F. Mann, B.A. Peppley, P.R. Roberge, Performance modeling of the Ballard Mark IV solid polymer electrolyte fuel cell, J. Electrochem. Soc. 142 (1995) 1–8.
[19] M.J. Khan, M.T. Iqbal, Modeling and analysis of electrochemical, thermal, and reactant flow dynamics for a PEM fuel cell system, Fuel Cells 5 (2005) 463–475.
[20] A.K.M.M. Murshed, B. Huang, K. Nandakumar, Control relevant modeling of planer solid oxide fuel cell system, J. Power Sources 163 (2007) 830–845.
[21] N. Lu, Q.L.X. Sun, M.A. Khaleel, The modeling of a standalone solid-oxide fuel auxiliary power unit, J. Power Sources 161 (2006) 938–948.
[22] E. Riensche, U. Stimming, G. Unverzagt, Optimization of a 200 kW SOFC cogeneration power plant Part I: Variation of process parameters, J. Power Sources 73 (1998) 251–256.
[23] M.N. Cirstea, A. Dinu, J.G. Khor, M. McCormick, Neural and Fuzzy Logic Control of Drives and Power Systems, Newnes, Oxford, 2002.
[24] A.J.B. Antunes, J.A.F.R. Pereira, A.M.F. Fileti, Fuzzy control of a PMMA batch reactor: development and experimental testing, Comp. Chem. Eng. 30 (2005) 268–276.
[25] J. Jantzen, Tuning of Fuzzy PID Controllers, Technical University of Denmark, Department of Automation, Lecture notes, 1998.